Supplement of

Temperature-dependent multiphase chemical kinetics can explain uniform atmospheric nanoparticle growth rates

Zhiqiang Zhang[1], Hyun Gu Kang[1], Ulrich Pöschl[1], and Thomas Berkemeier[1]

[1]Multiphase Chemistry Department, Max Planck Institute for Chemistry, Hahn-Meitner-Weg 1, 55128 Mainz, Germany

Correspondence: Thomas Berkemeier (t.berkemeier@mpic.de)

Supplementary Text

S1 Kinetic multilayer model of multiphase chemistry

We use the kinetic multilayer model of multiphase chemistry (KM3C) to explicitly treat gas phase diffusion, particle-phase bulk diffusion, and multiphase partitioning kinetics based on vapor pressures (Fig. S4). KM3C is built in the framework of the kinetic multilayer meta model (KM-MEMO, Mishra et al., 2025), which is a Matlab toolkit that simplifies kinetic model construction by automatically generating and executing systems of differential equations from well-defined input files. KM3C addresses possible limitations in surface-bulk mass transfer and bulk diffusion, and detailed descriptions of the model and its predecessors are described elsewhere (Shiraiwa et al., 2012; Berkemeier et al., 2020; Kang et al., 2026). The model consists of the following compartments: gas phase, near-surface gas phase, a sorption layer, a quasi-static surface layer (near-surface bulk layer), and the particle bulk, subdivided into several bulk layers. The model is initiated with a freshly-nucleated particle (diameter of 0.9 nm) containing non-volatile organic species. When modelling the CERN CLOUD laboratory data, we fix the concentrations of gaseous OOMs to the values reported in Stolzenburg et al. (2018). When modelling the field measurement data, we interpolate the concentrations reported in Stolzenburg et al. (2025) of gaseous OOMs and H_2SO_4 across several time intervals.

In this study, we use a volatility basis set (VBS) approach that categorizes molecules by their saturation mass concentrations at 298 K (C^*_{298}) into logarithmically spaced volatility bins (Donahue et al., 2006, 2014; Stolzenburg et al., 2022). KM3C treats each volatility bin as a representative chemical species. For the field measurement data, we use average molecular weights reported for each volatility bin. For the CERN CLOUD chamber data, we use a linear relationship of volatility and molecular weight that we derive from the field measurements in a molecular corridor plot (Table S1 and Fig. S5, Shiraiwa et al., 2014). The model corrects C^*_{298} for temperature with the Clausius-Clapeyron equation (Eq. S1) and the enthalpy of vaporization (ΔH_{vap}), where R is the gas constant. We calculate the ΔH_{vap} for each volatility bin using the empirical relationship between

C^*_{298} and ΔH_{vap} (Eq. S2) proposed by Epstein et al. (2010) and use the parameters from Stolzenburg et al. (2022). An upper limit of 200 kJ mol^{-1} is applied to ΔH_{vap} (Cappa and Jimenez, 2010).

$$C^*(T) = C^*_{298} \times \exp\left(-\frac{\Delta H_{\text{vap}}}{R}\left(\frac{1}{T} - \frac{1}{298}\right)\right) \tag{S1}$$

$$\Delta H_{\text{vap}} = -5.7 \times \log_{10}(C^*_{298}) + 129 \tag{S2}$$

The model describes the temperature-dependence of bulk diffusivity with a similar Arrhenius-type equation (Eq. S3) and an activation energy of diffusion ($E_{\text{a,dif}}$). Here, we use a value of $E_{\text{a,dif}}$ = 40 kJ mol^{-1}, which is consistent with that of sucrose-water solutions (Kiland et al., 2019).

$$D_b(T) = D_{\text{b,298}} \times \exp\left(-\frac{E_{\text{a,dif}}}{R}\left(\frac{1}{T} - \frac{1}{298}\right)\right) \tag{S3}$$

We note that $E_{\text{a,dif}}$ will likely increase towards more viscous organic matrices, leading to super-Arrhenius behavior when approaching the glass transition, a property well-known from studies of the viscosity of so-called fragile glass-formers (Angell, 1991). A more detailed description of the composition- and temperature-dependence of the diffusion coefficient in organic nanoparticle growth will be the subject of future studies.

S2 Mass transfer coefficients

In KM3C, diffusion limitations affect growth rates mostly by slowing surface-to-bulk transfer, i.e. the transition of a molecule between being surface-adsorbed and being absorbed into the particle bulk. The surface-to-bulk transfer rate is directly proportional to the diffusivity in the topmost bulk layer and inversely proportional to the vapor pressure of the transported molecule (Shiraiwa et al., 2012; Berkemeier et al., 2020). Based on absorptive partitioning theory (Pankow, 1994), the surface-to-bulk transfer rate coefficient (k_{sb}) is calculated with Eq. S4:

$$k_{\text{sb}} = k_{\text{bs}}\frac{k_{\text{d}}}{k_{\text{a}}} \times \frac{\sum[Y_i]_{\text{b1}} RT}{p_{\text{vap}} N_{\text{A}}} \tag{S4}$$

in which, k_{d} and k_{a} are the desorption and adsorption rate coefficients. $\sum[Y]_{\text{b1}}$ is the sum of the molecular concentrations of all species Y_i in the near-surface bulk layer. p_{vap} is the vapor pressure of the partitioning species, R is the gas constant, T is the temperature, and N_{A} is Avogadro's number. k_{bs} is the bulk-to-surface transfer rate coefficient and is calculated with Eq. S5, where D_{b} is the bulk diffusivity, δ_{s} is the depth of sorption layer, and δ_{b1} is the depth of the near-surface bulk layer.

$$k_{\text{bs}} = \frac{2D_{\text{b}}}{\delta_{\text{s}} + \delta_{\text{b1}}} \tag{S5}$$

We use a first-order adsorption rate coefficient (k_{a}, Eq. S6), where α and ω are the mass accommodation coefficient and the mean thermal velocity of the adsorbing molecule respectively. C_{g} and θ are the gas phase diffusion correction factor and the fractional surface coverage (Shiraiwa et al., 2012).

$$k_{\mathrm{a}} = C_{\mathrm{g}} \alpha \frac{\omega}{4} (1 - \theta) \tag{S6}$$

To obtain the total flow of adsorption F_{ads} (unit s^{-1}) of molecules to the particle surface, k_{a} is multiplied with the near-surface gas concentration [$\mathrm{Z_{gs}}$] and the collision cross section A_{p} of the particle (Pöschl et al., 2007). This effective collision surface area of the particle in KM3C is calculated using the particle radius plus the sorption layer, for which we assume a thickness of 0.639 nm, corresponding to organic matter with an average molar mass of 220 g mol^{-1} and density of 1.4 g cm^{-3}.

The first-order desorption rate coefficient (k_{d}, Eq. S7) is the inverse of the surface desorption lifetime (τ_{d}), where A_{des} is the pre-exponential factor ($A_{\mathrm{des}} = 10^{13}$) and E_{des} is the activation energy of desorption (Knopf et al., 2024). Using literature values, Knopf et al. (2024) found a relationship between the standard saturation vapor pressure $p_{\mathrm{vap,298}}$ and E_{des}, which is shown in Fig. S6 and depends on the molecular oxygen-to-carbon ratio (O:C). As the organic compounds condensing on nanoparticles are likely highly oxygenated, we use a parameterization that runs along the left boundary of the data in this study. Note, however, that the choice of τ_{d} was not sensitive in the model simulations unless much larger values were chosen.

$$k_{\mathrm{d}} = \frac{1}{\tau_{\mathrm{d}}} = A_{\mathrm{des}} \exp\left(\frac{-E_{\mathrm{des}}}{RT}\right) \tag{S7}$$

The model corrects the vapor pressures for the Kelvin effect (Seinfeld and Pandis, 2016) by multiplying the vapor pressures with the Kelvin term ($K(D_{\mathrm{p}})$, Eq. S8). Here, D_{p} is the diameter of the particle, and D_{K10} is the Kelvin diameter at which the curvature effect becomes important (Eq. S9).

$$K(D_{\mathrm{p}}) = 10^{(D_{K10}/D_{\mathrm{p}})} \tag{S8}$$

$$D_{K10}(T) = 4.8 \times (300 \times T^{-1}) \tag{S9}$$

In line with the results by Tröstl et al. (2016), we find the impact of the Kelvin term on the simulation results to be rather small.

S3 Adaptive layer resizing algorithm

KM3C adopts an adaptive layer resizing algorithm that dynamically splits layers when a layer grows too large and merges adjacent layers when they are too thin (Kang et al., 2026). This algorithm is able to account for concentration gradients

dynamically as particles grow (or shrink) and can prevent numerical stiffness that arises when layers deplete. As the particles grow, solvating molecules enter the near-surface bulk layer, which can trigger a split of that layer via the adaptive layer resizing algorithm. However, this split can lead to an artificial and sudden increase in particle growth as k_{sb} and k_{bs} increase when δ_{b1} decreases. To solve this problem, we implement a moving-boundary algorithm (Couvidat and Sartelet, 2015; Kang et al., 2026), which keeps the depth of the near-surface bulk layer constant by increasing mass transport from the near-surface bulk layer to the underlying bulk layer when the the near-surface bulk layer grows. The enhanced diffusion is calculated based on the molecular volume flow into the near-surface bulk layer. The near-surface bulk layer in KM3C adopts the role and properties of the quasi-static surface layer formalized and used in previous studies (Pöschl et al., 2007; Shiraiwa et al., 2012).

S4 Hyytiälä SMEAR II station field measurement data

Stolzenburg et al. (2025) reported field measurements of H_2SO_4, OOMs and nanoparticle growth at the SMEAR II station in the boreal forests of Hyytiälä, Finland from April 11th (3.8 °C, 50.7 % RH) and August 17th (17.5 °C, 49.9 % RH) of 2020 (Gonzalez Carracedo et al., 2022). The brown line and shadings in Fig. 1 in the main text shows the best estimate and uncertainty range of traditional model calculations. Shadings are obtained by shifting the volatility basis set by ± 1 bin. We use the same methodology for the uncertainty range of the KM3C model calculations. The authors also reported OOMs volatility distributions estimated using the identified molecular ion signals and a parameterization based on elemental ratios (Donahue et al., 2011). We use the reported ion masses for the molecular weights of the volatility bin species in KM3C (black and blue markers in Fig. S5).

S5 CERN CLOUD laboratory data

We use laboratory experimental data of dark α-pinene ozonolysis conducted at the Cosmics Leaving Outdoor Droplets (CLOUD) chamber at the European Organization for Nuclear Research (CERN) (Kirkby et al., 2011; Stolzenburg et al., 2018). Experiments were performed at three different temperatures (25, 5, and -25 °C). Proton transfer reaction (PTR3) and nitrate chemical ionization mass spectrometers (NO3-CIMS) were used to measure the gas-phase species. Stolzenburg et al. (2018) reported detailed chemical composition for three experiments, which we simulate with KM3C at the temperatures, median organic vapor concentrations and volatility distributions reported, displayed as square markers in Fig. 3 in the main text. Stolzenburg et al. (2018) did not report the specific ion masses, and we estimate the molecular weights for the products in the CLOUD experiments using the ion masses in Stolzenburg et al. (2025) (Table S1). These values are shown as the red circles in Figure S5. Colored bands in Fig. 2 in the main text are obtained by linearly scaling the condensable organic vapor concentrations in the model at the three respective temperatures (-25, 5, and 25°C) to obtain a series of model simulations at the same temperatures. In main text Fig. 2, we vary the bulk diffusion coefficient within the semi-solid phase state range (10^{-20} – 10^{-15} cm^2 s^{-1}) and scale with temperature to obtain the upper and lower boundaries of the colored bands. To obtain shaded regions in main text

Fig. 3, we scale the obtained growth rates by a factor of 3 to account for experimental uncertainties, possible differences in the ambient vapor composition compared to the CERN CLOUD measurements, and possible differences in particle phase state.

S6 Diffusion limitations affecting nanoparticle growth

KM3C is sensitive to the bulk diffusion coefficient, which we vary across the range characteristic for liquid to solid phases
105 (10^{-22} – 10^{-10} cm^2 s^{-1}). Nanoparticle growth is affected by lowered diffusivities in two ways: development of differential concentration gradients (i.e. different compounds exhibit concentration gradients of different strength and direction) and reduced surface-to-bulk transfer. Both lead to reduced condensation of relatively higher volatile compounds (SVOC, LVOC).

Supplementary Figures

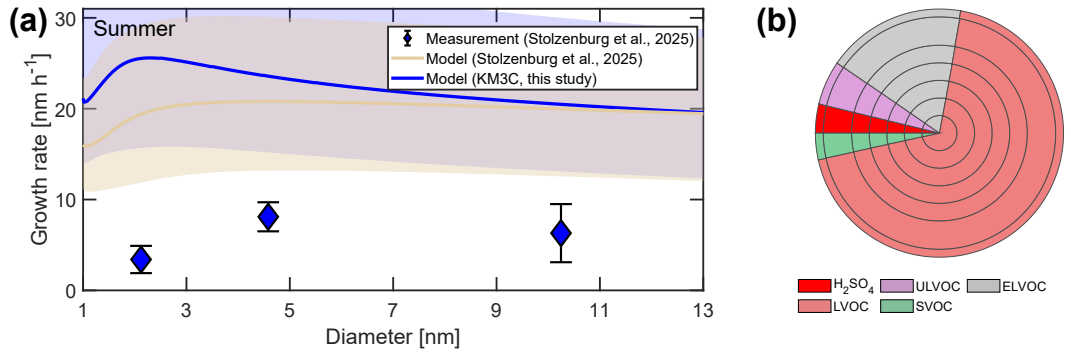

Figure S1. Observed and modelled atmospheric nanoparticle growth rates in a field experiment (Hyytiälä, 17th August, 2020). Same as Figs. 1a,c, but a higher diffusivity ($D_{\mathrm{b},298} = 1 \times 10^{-15}$ cm^2 s^{-1}) is utilized in KM3C modelling. **(a)** Observed growth rates (blue diamond markers and error bars representing arithmetic mean values and standard deviations) and vapor concentration-based predictions obtained with a two-film model (Stolzenburg et al., 2025, brown line and shading for best estimate and uncertainty range by shifting full VBS by $\pm$ 1 bin). The new multiphase kinetic model (KM3C; blue line and shading for best estimate and uncertainty range by shifting full VBS by $\pm$ 1 bin) predicts similar growth rates to Stolzenburg et al. (2025) but also overestimates the observed growth rates. **(b)** Higher diffusivity ($D_{\mathrm{b},298} = 1 \times 10^{-15}$ cm^2 s^{-1}) leads to well-mixed particles.

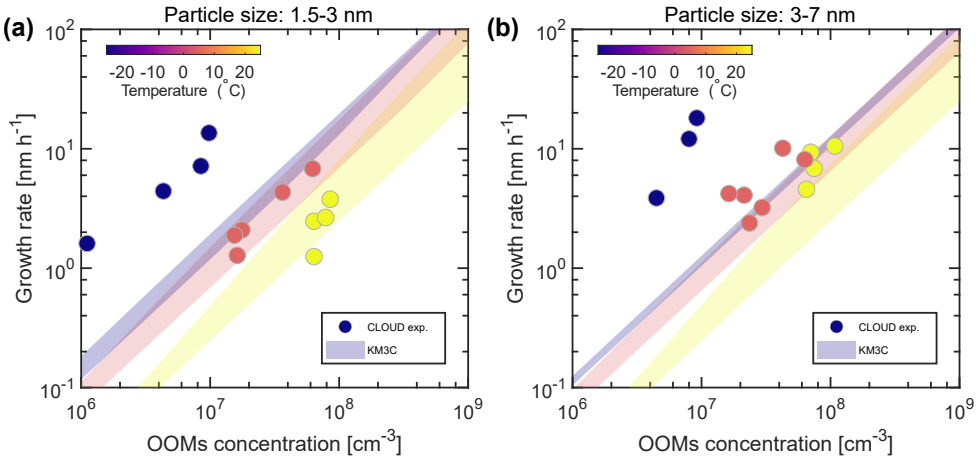

Figure S2. Nanoparticle growth rates in laboratory chamber experiments in the CERN CLOUD chamber and simulated with the KM3C kinetic model. Same as Fig. 2, but KM3C (colored bands) simulates nanoparticle growth rates for (a) 1.5-3 nm and (b) 3-7 nm using only the concentration of OOMs measured by NO3-CIMS data provided in Stolzenburg et al. (2018). Colored bands are obtained by linearly scaling the condensable organic material concentrations in the model at the three respective temperatures (-25, 5 and 25°C). Upper and lower boundaries of the shaded areas are obtained by varying the bulk diffusion coefficient $D_{b,298}$ within 10^{-20} – 10^{-15} cm^2 s^{-1} and detailed in Sect. S5.

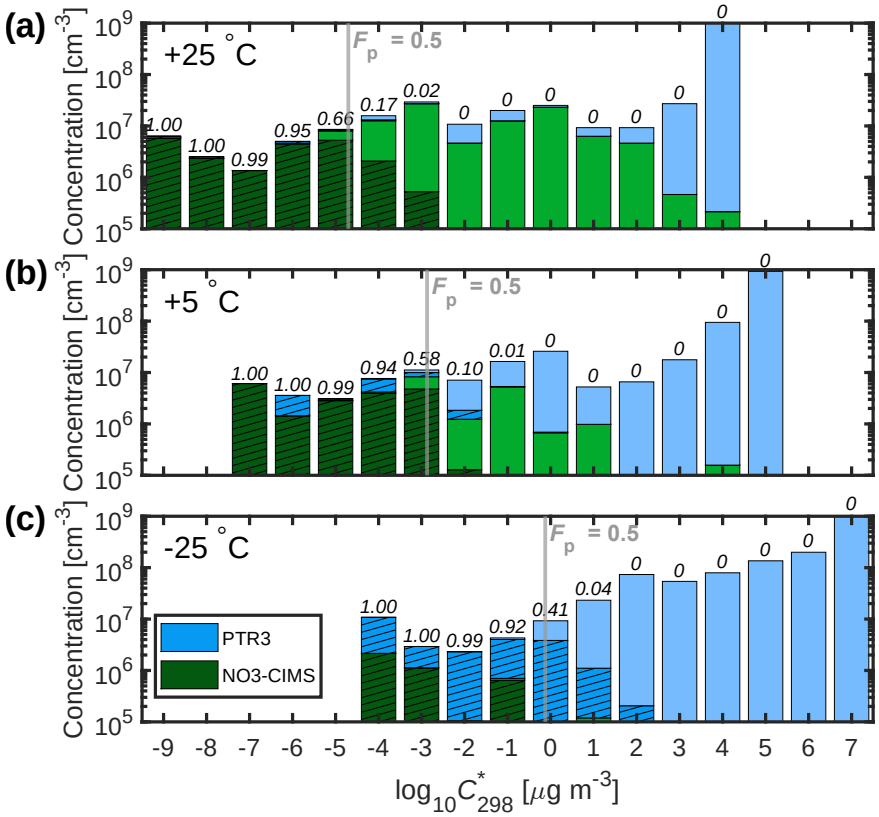

Figure S3. Volatility distributions of three experiments in the CERN CLOUD chamber. Experiments were conducted at **(a)** 25 °C, **(b)** 5 °C and **(c)** -25 °C reported by Stolzenburg et al. (2018). Shaded areas and numbers above the bars indicate fractions that partition into the particle phase (F_p) at an aerosol mass loading of 2×10^{-5} μg m^{-3} assuming equilibrium partitioning in a closed system (Pankow, 1994), corresponding to 10^3 particles cm^{-3} with 3 nm diameter, and the grey vertical lines indicate the volatility where F_p = 0.5.

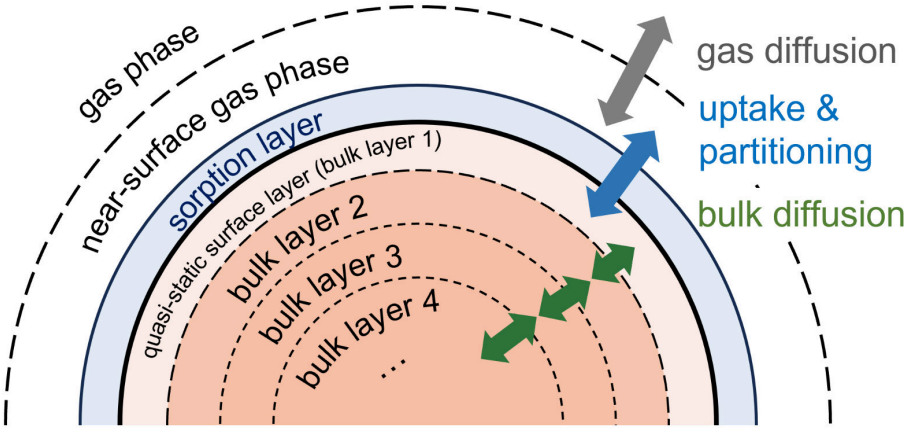

Figure S4. Overview of the kinetic multilayer model of multiphase chemistry (KM3C) used in this study. The particle bulk is subdivided into model layers to form concentration gradients and address slow diffusion.

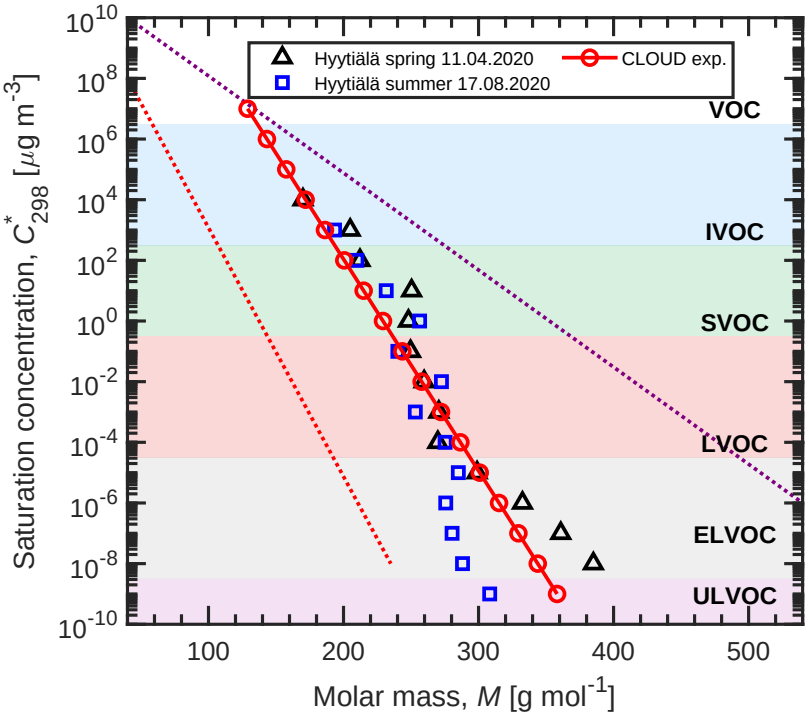

Figure S5. Molecular corridors of SOA evolution. KM3C incorporates volatility (298 K) and molar mass data from the field measurements in Hyytiälä, Finland, 11th April, 2020 (black triangles) and 17th August, 2020 (blue squares) in Stolzenburg et al. (2025). A linear relationship derived from these field measurements is applied to the CERN CLOUD chamber simulations (red circles).

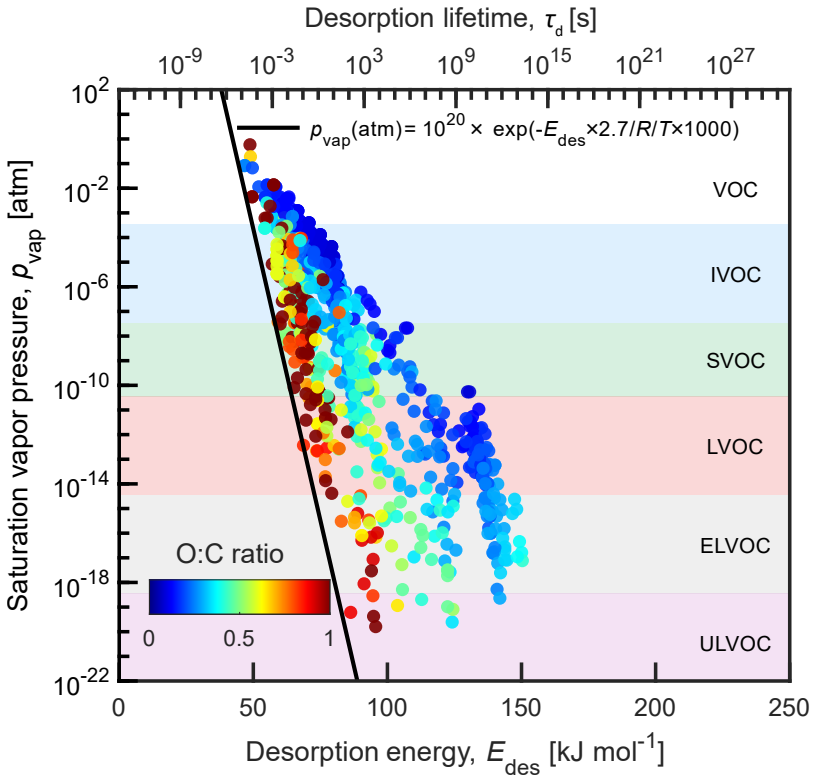

Figure S6. Relationship between saturation vapor pressure (p_{vap} at 298 K), desorption energies (E_{des}) implemented in KM3C. Desorption lifetime (τ_d) of species with a molar mass of 220 g mol^{-1} at 298 K is shown on the top axis. Markers indicate literature data (Knopf et al., 2024), where the colors show the O:C of the molecules. The black line is drawn using the shown equation, which is the parameterization used to retrieve E_{des} in KM3C.

Supplementary Tables

Table S1. Species measured in field measurements at a boreal forest site (Hyytiälä, Finland, 11 April and 17 August 2020) and in laboratory experiments (CERN CLOUD chamber), along with the volatility at 298 K and molar mass for each species used in KM3C in this study.

Species	Molar mass (Summer, g mol^{-1})	Molar mass (Spring, g mol^{-1})	Molar mass (CLOUD exp., g mol^{-1})
SOA (C^* = 10^7 μg m^{-3})	-	-	129
SOA (C^* = 10^6 μg m^{-3})	-	-	143
SOA (C^* = 10^5 μg m^{-3})	-	-	158
SOA (C^* = 10^4 μg m^{-3})	-	170	172
SOA (C^* = 10^3 μg m^{-3})	193	205	186
SOA (C^* = 10^2 μg m^{-3})	210	212	201
SOA (C^* = 10^1 μg m^{-3})	232	250	215
SOA (C^* = 10^0 μg m^{-3})	256	248	229
SOA (C^* = 10^{-1} μg m^{-3})	240	250	244
SOA (C^* = 10^{-2} μg m^{-3})	273	260	258
SOA (C^* = 10^{-3} μg m^{-3})	253	271	272
SOA (C^* = 10^{-4} μg m^{-3})	275	270	287
SOA (C^* = 10^{-5} μg m^{-3})	285	299	301
SOA (C^* = 10^{-6} μg m^{-3})	276	333	315
SOA (C^* = 10^{-7} μg m^{-3})	280	361	330
SOA (C^* = 10^{-8} μg m^{-3})	288	385	344
SOA (C^* = 10^{-9} μg m^{-3})	308	-	358
SOA (non-volatile) [a]	308	385	358
H_2SO_4 [b]	98	98	-

[a] Species in pre-existing nanoparticles are assumed to be non-volatile and are grouped into ULVOC in this study, and the molar mass of them are assumed to be the same as species in the lowest volatility bin.

[b] H_2SO_4 is assumed to have negligible vapor pressure following the assumption in the previous literature (Nieminen et al., 2010; Häkkinen et al., 2013).

References

Angell, C.: Relaxation in liquids, polymers and plastic crystals — strong/fragile patterns and problems, J. Non-Cryst. Solids, 131-133, 13–31, https://doi.org/https://doi.org/10.1016/0022-3093(91)90266-9, 1991.

Berkemeier, T., Takeuchi, M., Eris, G., and Ng, N. L.: Kinetic modeling of formation and evaporation of secondary organic aerosol from NO_3 oxidation of pure and mixed monoterpenes, Atmos. Chem. Phys., 20, 15 513–15 535, https://doi.org/10.5194/acp-20-15513-2020, 2020.

Cappa, C. D. and Jimenez, J. L.: Quantitative estimates of the volatility of ambient organic aerosol, Atmos. Chem. Phys., 10, 5409–5424, https://doi.org/10.5194/acp-10-5409-2010, 2010.

Couvidat, F. and Sartelet, K.: The Secondary Organic Aerosol Processor (SOAP v1.0) model: a unified model with different ranges of complexity based on the molecular surrogate approach, Geosci. Model Dev., 8, 1111–1138, https://doi.org/10.5194/gmd-8-1111-2015, 2015.

Donahue, N. M., Robinson, A. L., Stanier, C. O., and Pandis, S. N.: Coupled Partitioning, Dilution, and Chemical Aging of Semivolatile Organics, Environ. Sci. Technol., 40, 2635–2643, https://doi.org/10.1021/es052297c, 2006.

Donahue, N. M., Epstein, S. A., Pandis, S. N., and Robinson, A. L.: A two-dimensional volatility basis set: 1. organic-aerosol mixing thermodynamics, Atmos. Chem. Phys., 11, 3303–3318, https://doi.org/10.5194/acp-11-3303-2011, 2011.

Donahue, N. M., Robinson, A. L., Trump, E. R., Riipinen, I., and Kroll, J. H.: Volatility and Aging of Atmospheric Organic Aerosol, in: Atmospheric and Aerosol Chemistry, edited by McNeill, V. F. and Ariya, P. A., Topics in Current Chemistry, pp. 97–143, Springer, Berlin, Heidelberg, https://doi.org/10.1007/128_2012_355, 2014.

Epstein, S. A., Riipinen, I., and Donahue, N. M.: A Semiempirical Correlation between Enthalpy of Vaporization and Saturation Concentration for Organic Aerosol, Environ. Sci. Technol., 44, 743–748, https://doi.org/10.1021/es902497z, pMID: 20025284, 2010.

Gonzalez Carracedo, L., Lehtipalo, K., Ahonen, L. R., Sarnela, N., Holm, S., Kangasluoma, J., Kulmala, M., Winkler, P. M., and Stolzenburg, D.: On the relation between apparent ion and total particle growth rates in the boreal forest and related chamber experiments, Atmos. Chem. Phys., 22, 13 153–13 166, https://doi.org/10.5194/acp-22-13153-2022, 2022.

Häkkinen, S. A. K., Manninen, H. E., Yli-Juuti, T., Merikanto, J., Kajos, M. K., Nieminen, T., D'Andrea, S. D., Asmi, A., Pierce, J. R., Kulmala, M., and Riipinen, I.: Semi-empirical parameterization of size-dependent atmospheric nanoparticle growth in continental environments, Atmos. Chem. Phys., 13, 7665–7682, https://doi.org/10.5194/acp-13-7665-2013, 2013.

Kang, H. G., Takeuchi, M., Ng, N. L., Pöschl, U., and Berkemeier, T.: Multiphase Chemistry and Phase State Explain Nonlinear Effects in the Formation and Evaporation of SOA from Mixed Monoterpene Precursors, ACS ES&T Air, https://doi.org/10.1021/acsestair.5c00438, 2026.

Kiland, K. J., Maclean, A. M., Kamal, S., and Bertram, A. K.: Diffusion of Organic Molecules as a Function of Temperature in a Sucrose Matrix (a Proxy for Secondary Organic Aerosol), J. Phys. Chem. Lett., 10, 5902–5908, https://doi.org/10.1021/acs.jpclett.9b02182, 2019.

Kirkby, J., Curtius, J., Almeida, J., Dunne, E., Duplissy, J., Ehrhart, S., Franchin, A., Gagné, S., Ickes, L., Kürten, A., Kupc, A., Metzger, A., Riccobono, F., Rondo, L., Schobesberger, S., Tsagkogeorgas, G., Wimmer, D., Amorim, A., Bianchi, F., Breitenlechner, M., David, A., Dommen, J., Downard, A., Ehn, M., Flagan, R. C., Haider, S., Hansel, A., Hauser, D., Jud, W., Junninen, H., Kreissl, F., Kvashin, A., Laaksonen, A., Lehtipalo, K., Lima, J., Lovejoy, E. R., Makhmutov, V., Mathot, S., Mikkilä, J., Minginette, P., Mogo, S., Nieminen, T., Onnela, A., Pereira, P., Petäjä, T., Schnitzhofer, R., Seinfeld, J. H., Sipilä, M., Stozhkov, Y., Stratmann, F., Tomé, A., Vanhanen, J., Viisanen, Y., Vrtala, A., Wagner, P. E., Walther, H., Weingartner, E., Wex, H., Winkler, P. M., Carslaw, K. S., Worsnop, D. R., Baltensperger,

U., and Kulmala, M.: Role of sulphuric acid, ammonia and galactic cosmic rays in atmospheric aerosol nucleation, Nature, 476, 429–433, https://doi.org/10.1038/nature10343, 2011.

Knopf, D. A., Ammann, M., Berkemeier, T., Pöschl, U., and Shiraiwa, M.: Desorption lifetimes and activation energies influencing gas–surface interactions and multiphase chemical kinetics, Atmos. Chem. Phys., 24, 3445–3528, https://doi.org/10.5194/acp-24-3445-2024, 2024.

Mishra, A., Kilchhofer, K., Iezzi, L., Pöschl, U., Alpert, P. A., Ammann, M., and Berkemeier, T.: Photochemical Degradation of Iron Citrate in Anoxic Viscous Films Enhanced by Redox Cascades, ACS Earth Space Chem., 9, 689–698, https://doi.org/10.1021/acsearthspacechem.4c00364, 2025.

Nieminen, T., Lehtinen, K. E. J., and Kulmala, M.: Sub-10 nm particle growth by vapor condensation – effects of vapor molecule size and particle thermal speed, Atmos. Chem. Phys., 10, 9773–9779, https://doi.org/10.5194/acp-10-9773-2010, 2010.

Pankow, J. F.: An absorption model of the gas/aerosol partitioning involved in the formation of secondary organic aerosol, Atmos. Environ., 28, 189–193, https://doi.org/10.1016/1352-2310(94)90094-9, 1994.

Pöschl, U., Rudich, Y., and Ammann, M.: Kinetic model framework for aerosol and cloud surface chemistry and gas-particle interactions ndash; Part 1: General equations, parameters, and terminology, Atmos. Chem. Phys., 7, 5989–6023, https://doi.org/10.5194/acp-7-5989-2007, 2007.

Seinfeld, J. H. and Pandis, S. N.: Atmospheric chemistry and physics: from air pollution to climate change, John Wiley & Sons, 2016.

Shiraiwa, M., Pfrang, C., Koop, T., and Pöschl, U.: Kinetic multi-layer model of gas-particle interactions in aerosols and clouds (KM-GAP): linking condensation, evaporation and chemical reactions of organics, oxidants and water, Atmos. Chem. Phys., 12, 2777–2794, https://doi.org/10.5194/acp-12-2777-2012, 2012.

Shiraiwa, M., Berkemeier, T., Schilling-Fahnestock, K. A., Seinfeld, J. H., and Pöschl, U.: Molecular corridors and kinetic regimes in the multiphase chemical evolution of secondary organic aerosol, Atmos. Chem. Phys., 14, 8323–8341, https://doi.org/10.5194/acp-14-8323-2014, 2014.

Stolzenburg, D., Fischer, L., Vogel, A. L., Heinritzi, M., Schervish, M., Simon, M., Wagner, A. C., Dada, L., Ahonen, L. R., Amorim, A., Baccarini, A., Bauer, P. S., Baumgartner, B., Bergen, A., Bianchi, F., Breitenlechner, M., Brilke, S., Buenrostro Mazon, S., Chen, D., Dias, A., Draper, D. C., Duplissy, J., El Haddad, I., Finkenzeller, H., Frege, C., Fuchs, C., Garmash, O., Gordon, H., He, X., Helm, J., Hofbauer, V., Hoyle, C. R., Kim, C., Kirkby, J., Kontkanen, J., Kürten, A., Lampilahti, J., Lawler, M., Lehtipalo, K., Leiminger, M., Mai, H., Mathot, S., Mentler, B., Molteni, U., Nie, W., Nieminen, T., Nowak, J. B., Ojdanic, A., Onnela, A., Passananti, M., Petäjä, T., Quéléver, L. L. J., Rissanen, M. P., Sarnela, N., Schallhart, S., Tauber, C., Tomé, A., Wagner, R., Wang, M., Weitz, L., Wimmer, D., Xiao, M., Yan, C., Ye, P., Zha, Q., Baltensperger, U., Curtius, J., Dommen, J., Flagan, R. C., Kulmala, M., Smith, J. N., Worsnop, D. R., Hansel, A., Donahue, N. M., and Winkler, P. M.: Rapid growth of organic aerosol nanoparticles over a wide tropospheric temperature range, P. Natl. Acad. Sci. USA, 115, 9122–9127, https://doi.org/10.1073/pnas.1807604115, 2018.

Stolzenburg, D., Wang, M., Schervish, M., and Donahue, N. M.: Tutorial: Dynamic organic growth modeling with a volatility basis set, J. Aerosol Sci., 166, 106 063, https://doi.org/10.1016/j.jaerosci.2022.106063, 2022.

Stolzenburg, D., Sarnela, N., Bianchi, F., Cai, J., Cai, R., Cheng, Y., Dada, L., Donahue, N. M., Grothe, H., Holm, S., Kerminen, V.-M., Lehtipalo, K., Petäjä, T., Sulo, J., Winkler, P. M., Yan, C., Kangasluoma, J., and Kulmala, M.: Incomplete mass closure in atmospheric nanoparticle growth, npj Clim. Atmos. Sci., 8, https://doi.org/10.1038/s41612-025-00893-5, 2025.

Tröstl, J., Chuang, W. K., Gordon, H., Heinritzi, M., Yan, C., Molteni, U., Ahlm, L., Frege, C., Bianchi, F., Wagner, R., Simon, M., Lehtipalo, K., Williamson, C., Craven, J. S., Duplissy, J., Adamov, A., Almeida, J., Bernhammer, A.-K., Breitenlechner, M., Brilke, S., Dias, A.,

Ehrhart, S., Flagan, R. C., Franchin, A., Fuchs, C., Guida, R., Gysel, M., Hansel, A., Hoyle, C. R., Jokinen, T., Junninen, H., Kangasluoma,
185 J., Keskinen, H., Kim, J., Krapf, M., Kürten, A., Laaksonen, A., Lawler, M., Leiminger, M., Mathot, S., Möhler, O., Nieminen, T., Onnela, A., Petäjä, T., Piel, F. M., Miettinen, P., Rissanen, M. P., Rondo, L., Sarnela, N., Schobesberger, S., Sengupta, K., Sipilä, M., Smith, J. N., Steiner, G., Tomè, A., Virtanen, A., Wagner, A. C., Weingartner, E., Wimmer, D., Winkler, P. M., Ye, P., Carslaw, K. S., Curtius, J., Dommen, J., Kirkby, J., Kulmala, M., Riipinen, I., Worsnop, D. R., Donahue, N. M., and Baltensperger, U.: The role of low-volatility organic compounds in initial particle growth in the atmosphere, Nature, 533, 527–531, https://doi.org/10.1038/nature18271, 2016.